Advances in Thermal Processes and Energy Transformation
Volume 8, 2025, MUZY01, pp. 1-8, ISSN 2585-9102
https://doi.org/10.54570/atpet2025/08/01/0001

Analysis of CFD Modelling Results of Designed Uniflow Vortex Tube Models

Ihor Muzychka[1] ● Jan Kizek[1] ● Andriy Menkov[2] ● Yevhen Karakash[3] ● Andrii Kulikov[1]

[1]Department of Process Engineering, Technical University of Košice, Faculty of Manufacturing Technologies with a seat in Prešov, Bayerova 1, 080 01 Prešov, Slovak Republic, ihor.muzychka@tuke.sk, jan.kizek@tuke.sk, andrii.kulikov@tuke.sk
[2] Head of production R&D Skyrora Ltd., 7 Drum Mains Park, Cumbernauld, Glasgow G68 9LD, United Kingdom, andrey.menkov@skyrora.com
[3] Dnipro Metallurgical Institute, Ukrainian State University of Science and Technologies, Lazaryana Street 2, 49010 Dnipro, Ukraine, yevgenkarakash@gmail.com

Category : Original Scientific Paper
Received : 3 March 2025 / Revised: 25 March 2025 / Accepted: 26 March 2025

Keywords: CFD modelling, Compressed air, Energy separation, Ranque-Hilsch vortex effect, Uniflow Vortex tube

Abstract: This study presents the results of CFD modelling of a uniflow Vortex tube based on the Ranque-Hilsch effect. The designed models are based on experimental measurements and calculations presented in [1], with the calculations derived from relationships published by Takahama [2] and Soni [3]. The tube geometry was designed according to these relationships for an inlet pressure of 0.5 MPa, which was also used in the CFD simulations. Two different inlet air geometries were tested. The analysis focused on velocity and temperature fields in the developed mathematical models. The results will serve as a basis for the design of experimental devices.

Citation: Muzychka Ihor, Kizek Jan, Menkov Andriy, Karakash Yevhen, Kulikov Andrii: Analysis of CFD Modelling Results of Designed Uniflow Vortex Tube Models, Advance in Thermal Processes and Energy Transformation, Volume 8, No.1 (2025), pp. 1-8, ISSN 2585-9102. https://doi.org/10.54570/atpet2025/08/01/0001

1 Introduction

In an effort to find alternative energy sources that do not harm the environment, experts are turning their attention to vortex energy. Nikola Tesla was the first well-known scientist to draw humanity's attention to the need for unconventional approaches in energy production. In 1892, he expressed the following view: “We are moving at an incomprehensible speed through infinite space. Everything around us is in motion, and energy is everywhere. There must be a more direct way to harness this energy than is currently known. When light comes from the environment around us, and when all forms of energy are effortlessly obtained from this inexhaustible source in the same way, humanity will advance by leaps and bounds” [4].

Currently, many countries utilize devices based on the Ranque-Hilsch effect, known as Vortex tubes (VT) or Ranque-Hilsch Vortex tubes (RHVT).

The Ranque-Hilsch Vortex tube (RHVT) is a device that enables temperature separation in a stream of compressed gas without the need for moving parts. This phenomenon was first observed by G. J. Ranque in 1930, and in 1934, he obtained an American patent for his discovery [1]. Subsequently, R. Hilsch conducted a more detailed investigation of the issue, publishing an extensive analysis of the physical principles of this process in 1947 [2]. Since its discovery, the RHVT has been used in a wide range of technical applications, particularly in industrial automation, cryogenics, and thermal management, where it facilitates localized cooling or heating without requiring external energy sources.

Research in this field to date has led to the development of several design variants of the RHVT. Based on experimental studies, mathematical relationships have been derived to optimize the tube's geometry in relation to the physical parameters of the gaseous medium. However, these relationships have primarily focused on counter-flow RHVTs [2,3,6-9], with most publications stating that the ratio of the tube's length L_{vt} to its internal diameter D_{vt} should be in the range of $20 < L_{vt}/D_{vt} < 55.5$, or more is mentioned if this ratio is ≥ 32 [3].

One of the less-explored RHVT variants is the uniflow configuration, also known as the parallel flow or co-flow tube. This version has been described in several studies [10-13], but it has not yet gained widespread practical use. The aim of this work is to design the geometry of a uniflow RHVT based on available information from existing literature and to create a mathematical model for its simulation using CFD software. The geometry design is based on mathematical relationships derived for counter-flow RHVTs. Autodesk® Simulation CFD 2021 was used for simulations, and Autodesk® Inventor 2021 was employed for the structural design. Two uniflow models with different geometries of the compressed air inlet stream were created. The analysis focuses on the separation of the incoming air into two fractions using the vortex effect and on comparing the flow properties and performance depending on various geometric and physical parameters of the medium.

2 Materials and methods

The geometric aspects concern the proper placement of the compressed gas inlet nozzle, the positioning of the hot and cold outlets, the tube length, the diameter of the vortex chamber, the tube, the outlet diameters, the angle of the incoming gas, and the shape of the control valve (needle) at the hot end. Hilsch was the first to investigate the influence of the placement and size of individual components on the performance of the tube [14].

Regarding the correct placement of the cold outlet for the tube, Ranque proposed two possible solutions [6].

Similar to Figure 1, one possible configuration of the VT is where the cold outlet is positioned on the same side as the hot outlet.

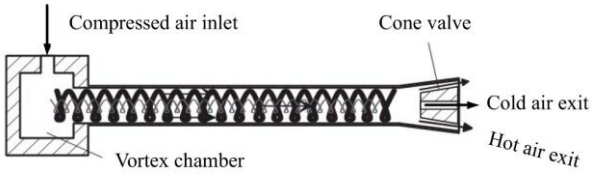

Figure 1 Schematic diagram of vortex tube.[6]

Numerous experiments have shown that a counter-flow vortex tube is generally more effective [5,6].

Linderstrom-Lang analysed the influence of the position of the control needle and the shape of the inlet nozzle on the flow characteristics of compressed gas [8].

In 1955, Westley experimentally optimized the geometric parameters of the vortex tube to improve its functionality and efficiency. He found that optimal performance could be achieved through an appropriate combination of inlet region, tube length, dimensions of the vortex chamber, cold zone, cold air outlet, and inlet pressure [9]. The resulting ratios are presented in [1, 15].

In the 1960s, Takaham proposed a different mathematical relationship for determining the optimal geometry of a vortex tube. He discovered that if the Mach number at the inlet reaches a value in the range of 0.5 to 1, the vortex tube geometry should correspond to the relationship described in [2,15], as such a configuration allows for a more pronounced heating and cooling effect.

In his study [3], Soni presented the results of experiments conducted on more than 170 different vortex tube configurations, identifying the optimal performance that can be achieved by following the defined geometric relationships presented in [1,3,15,16].

Available findings indicate that all previously described geometric relationships for vortex tubes share common fundamental characteristics. These relationships were subsequently experimentally verified by Raisky [17] in 1974.

2.1 Design of the Vortex tube geometry

The construction of a vortex tube largely depends on its overall length, geometric parameters, and the configuration of its individual components. The main parts of the Vortex tube (VT), whose geometry significantly affects the flow behaviour and temperature separation effect, include: the inlet nozzle (often designed in the shape of an Archimedean spiral), hot and cold gas outlets, the regulating element (cone or needle), the vortex chamber, and the main tube body. Review publications such as [10,15,18-20] present various VT geometries that have been investigated by numerous authors through both experimental studies and mathematical modelling.

For the cold and hot air outlets, a truncated regulator was selected, as illustrated in Figure 2.

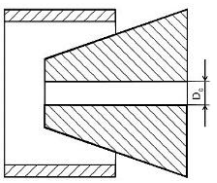

Figure 2 Schematic of uniflow VT outlet – Cone valve

The diameter for the cold outlet D_c will be determined based on calculations according to [1], as

well as the selected VT parameters and the corresponding calculated values, which will be presented in the relevant tables.

Theoretically, the expansion angle of the cone valve ranges between 45° and 60°. In this model, an angle of 60° is selected to allow a smoother transition from the vortex to the outlet. An opening for the cold fraction is located along the axis of the cone valve. A gap is created between the inner wall of the vortex tube and the cone valve to allow the discharge of the hot fraction. This arrangement provides the conditions necessary for the tube to operate on the uniflow principle.

2.1.1 Model 1: Geometry and CFD Setup

For the design of Model 1, the inlet pressure of compressed air was set to 500 kPa, with a ratio of L_{vt}/D_{vt} = 45.

Air is supplied to the system through a nozzle of optimal diameter, aiming to minimize pressure loss. A nozzle that is too narrow may result in significant pressure drop, while an excessively large diameter will not generate the required vortex motion.

In Model 1, the inlet nozzle is implemented as a 20 mm long tube mounted in the body of the vortex tube at an angle of 80° relative to its axis, in order to prevent reverse vortex flow.

Based on the relationships proposed by Takahama [2], the calculated optimal nozzle diameter is 6 mm.

The geometric design of Model No. 1 is illustrated in Figure 3.

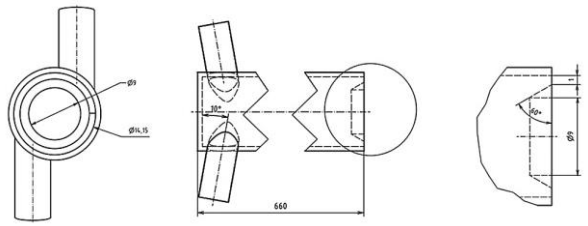

Figure 3 Input configuration schematic – Model 1

The calculated VT parameters obtained according to the relations in [1], which are based on the works [2,3,9], are presented in Table 1.

Table 1 Geometrical parameters for Model 1.

L_{vt}	D_{vt}	A_{vt}	D_{in}	A_{in}	D_{co}	A_{co}
mm	mm	mm^2	mm	mm^2	mm	mm^2
660	14.15	157.5	6	28.26	9	65

L_{vt}- length of the vortex tube, (m)
D_{vt}- diameter of the vortex tube, (m)
A_{vt} – area of the vortex tube, (m^2)
D_{in}- diameter of the inlet nozzle, (m)
A_{in} – area of the inlet nozzle (m^2)
D_c- diameter of the cold outlet nozzle, (m)
A_c – flow area at the cold outlet, (m^2)

Based on the calculated parameters of the proposed vortex tube design, a three-dimensional model was developed using Autodesk® Inventor 2021. This geometry was subsequently imported into Autodesk® Simulation CFD 2021 to construct the computational domain for numerical analysis. A discretized mesh was generated, material properties were assigned, and appropriate boundary conditions were defined in accordance with [21]. These steps enabled the simulation of the vortex effect under the specified flow conditions.

Table 2 Boundary conditions for Model 1.

Condition type	*Input/Output/Wall*
Gliding / Symmetry	Wall
Heat transfer coefficient (20 W.m^{-2}.K^{-1}, 20°C)	Wall
Pressure (500 kPa)	Input
Temperature (40°C)	Input
Pressure (0 Pa)	Output

In Table 2, the parameters required for simulation setup are listed. Pressure values are expressed as gauge pressure relative to the ambient pressure, defined here as p_0 = 101325 Pa (standard atmospheric pressure).

Among the available turbulence models, the SST k-ω RC (Shear Stress Transport k-omega with Rotation and Curvature correction) model developed by Smirnov and Menter [22] was selected for the simulation. This model is recommended for flows with significant curvature, such as those commonly encountered in cyclone separators. It is a two-equation model enhanced with corrections for rotation and curvature (RC), which increases its computational complexity and requires finer mesh resolution.

The compressibility of the working fluid was considered during the simulation setup.

The computational mesh was generated using the Autosize function, resulting in a total of 101,429 nodes and 499,901 elements.

One of the advantages of the model is its accurate numerical transport mechanism for scalar quantities such as velocity and temperature across the solution domain. Autodesk® CFD provides five advection schemes [23], of which the ADV 5 scheme (a modified Petrov–Galerkin formulation) was employed in this study for its superior stability and accuracy.

2.1.2 Model 2: Geometry and CFD Setup

The previous model exhibited a limitation in that the calculated length of the device was such that the vortex motion inside the tube could not maintain its structure for a sufficient duration. Consequently, the flow became mixed prior to reaching the outlet, resulting in the loss

of the heat separation effect. The proposed solution to this issue involved reducing the tube length and recalculating the remaining parameters inversely.

For further modelling, an adjustment to the L_{vt} parameter was considered, specifically a 10-fold reduction in its length. Simultaneously, the L_{vt}/D_{vt} ratio was modified to 32, thereby increasing the internal diameter of the tube. These modifications comply with the minimum design requirements for a vortex tube (VT) as recommended by various authors in the literature.

Model 2 was designed with a modified compressed air inlet. To enhance vortex flow at the inlet, the use of six nozzles was proposed, as depicted in Figure 4.

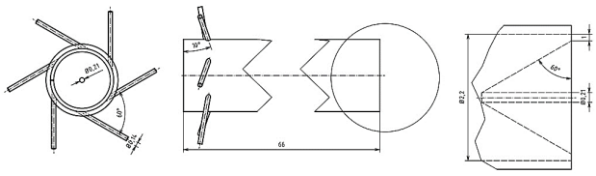

Figure 4 Input configuration schematic – Model 2

The VT parameters calculated for Model 2, based on the relations in [1] and derived from the works [2,3,9], are presented in Table 3.

Table 3 Geometrical parameters for Model 2.

L_{vt}	D_{vt}	A_{vt}	D_{in}	A_{in}	D_{co}	A_{co}
mm	mm	mm^2	mm	mm^2	mm	mm^2
66	2.2	3.8	0.14	0.0154	0.21	0.035

The geometry of the 3D Model 2 was constructed using Autodesk® Inventor 2021 software. The resulting model serves as the foundation for a simulation model in Autodesk® Simulation CFD 2021. The initial simulation parameters were maintained consistent with those applied to the first model. Due to the modification of the geometry, the dimensions of the computational mesh were altered. The mesh for numerical computations was generated using the Autosize function. To address the task, a total of 78,146 nodes and 356,199 elements were created.

3 Results and discussion

3.1 Simulation Results for Model 1

For Model No.1, the simulation process comprised 1498 iterations. Convergence was achieved when successive iterations produced negligible changes in the results, upon which the solver automatically terminated the computation. The average computational time per iteration was approximately 63 seconds.

To enable the simulation of airflow within the tube, all solid components of the model must be geometrically connected. The node incorporating the cone valve inside the tube imposes a significant computational load. To optimize solver performance, a small artificial connection was introduced between the cone valve and the tube wall. This modification is located at the downstream end of the tube – specifically at the outlet region of both the hot and cold streams. While this adjustment slightly disturbs the local vortex structure, it has negligible impact on overall heat transfer, as it is positioned at the boundary of the computational domain.

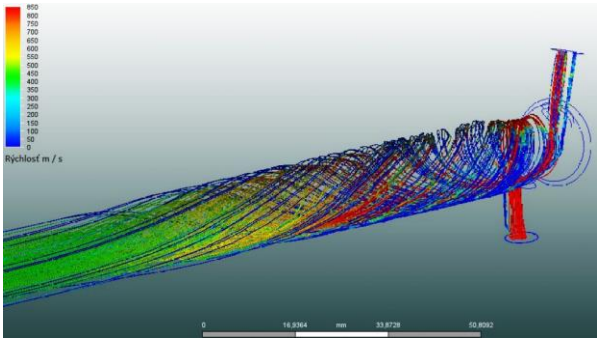

Figure 5 Velocity field with streamlines at inlet and tube body - Model 1

Figure 5 shows the visualization of the velocity field along airflow streamlines at the inlet and within the vortex tube of Model 1.

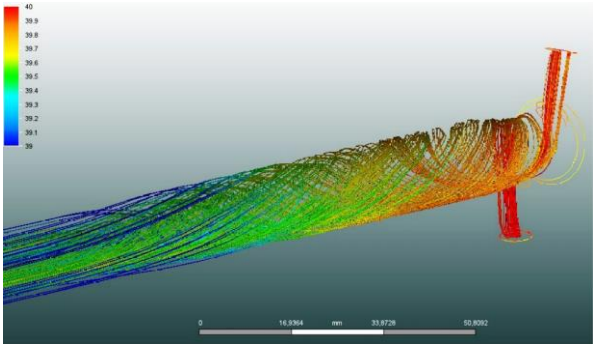

Figure 6 Inlet and tube temperature field streamlines – Model 1

Figure 6 shows the visualization of the temperature field along airflow streamlines at the inlet and within the vortex tube model of Model 1.

From Figures 5 and 6, it is evident that the compressed airflow supplied through the inlet nozzles generates a vortex flow, although the streamline structure remains intact only within the range of 0–15 cm. Analysis of the simulation results at the tube's inlet also indicates low heat transfer and limited separation of the hot and cold fractions of the swirling airflow. The flow behaviour changes at the tube's outlet. The subsequent Figures 7 and 8 illustrate the velocity trajectories and temperature variations along streamlines at the tube's end, respectively.

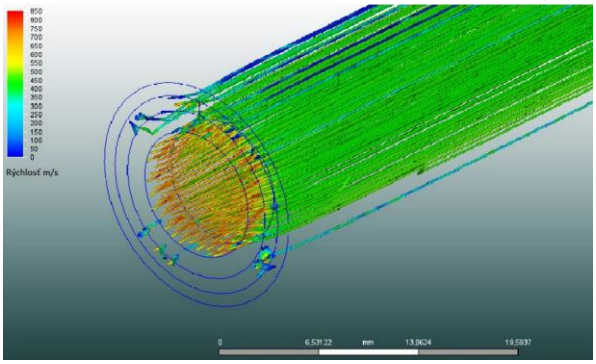

Figure 7 Velocity field with streamlines at the outlet and tube body - Model 1

Figure 7 illustrates the distribution of the velocity field along airflow streamlines at the outlet and within the vortex tube of Model 1. A comparison of the simulation results and streamline visualizations in Figures 5 and 7 reveals a transition from swirling to longitudinal flow, with an expected reduction in velocity near the inner wall of the vortex tube at its outlet end.

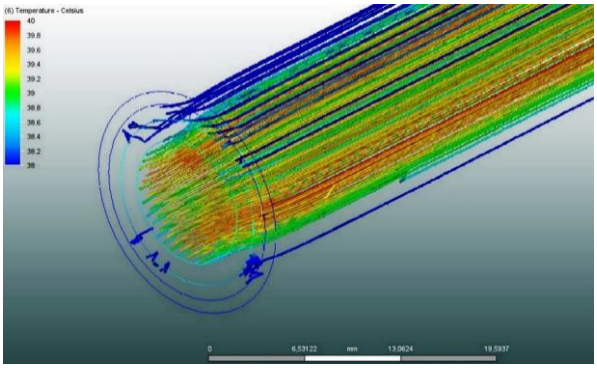

Figure 8 Temperature field with streamlines at the outlet and tube body - Model 1

Figure 8 presents the visualization of the temperature field along airflow streamlines at the outlet of Model 1. Analysis of the streamlines reveals partial separation of the hot and cold airflow streams. However, as noted in the flow analysis, the loss of swirling motion toward the tube's end, also observed in Figure 6, results in insufficient separation of the hot and cold fractions. This phenomenon indicates that the current simulation of Model 1 exhibits limitations in achieving effective temperature separation. To improve the performance of this vortex tube design, it is necessary to optimize the inlet parameters of the flowing medium to sustain swirling motion along the entire length of the tube, thereby enhancing the separation of cold and hot streams at the outlet of the proposed Model 1 geometry.

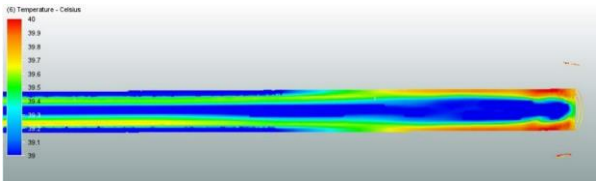

Figure 9 Temperature separation of flow fractions along the Vortex tube - Model 1

Figure 9 visualizes the temperature separation of hot and cold flow fractions along the length of the vortex tube in Model 1. The swirling effect diminishes before reaching the tube's outlet, resulting in cooler air being present at the expected hot outlet. This is attributed to the heat transfer conditions imposed at the outer flow boundaries, which cause the core flow to remain warmer than the periphery. In the swirling region depicted in Figure 9, the theoretically predicted thermal separation is observed, indicating that the anticipated vortex effect is partially achieved. However, the incomplete persistence of swirling motion suggests that further optimization of the inlet conditions is required to enhance separation efficiency across the entire tube length.

3.2 Simulation Results for Model 2

The simulation process for Model 2 was conducted under identical inlet medium parameters as Model 1. The simulation computation required 2253 iterations, representing a 50.4% increase compared to Model 1. Convergence was achieved when successive iterations yielded negligible changes in the results, at which point the solver terminated automatically. The average computational time per iteration was 42 seconds, approximately one-third shorter than that for Model 1, indicating improved computational efficiency per iteration despite the higher total iteration count.

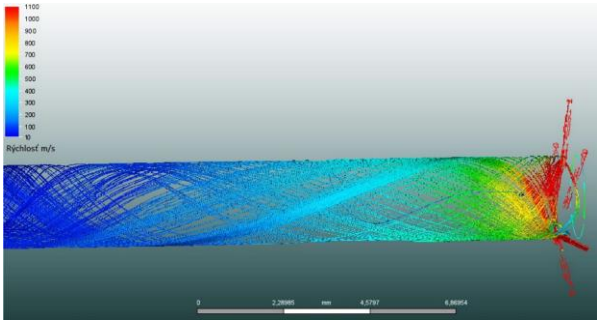

Figure 10 Velocity field with streamlines at inlet and tube body - Model 2

Figure 10 visualizes the velocity field along streamlines for Model 2, demonstrating that the swirling motion of the flow is maintained along the length of the vortex tube.

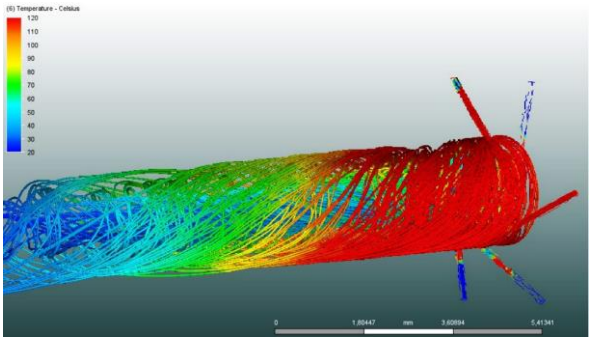

Figure 11 Inlet and tube temperature field streamlines – Model 2

Figure 11 visualizes the temperature field along streamlines for Model 2, from the inlet through the swirling nozzles. The simulation analysis reveals the separation of hot and cold flow fractions, consistent with the sustained swirling motion observed in Figure 10.

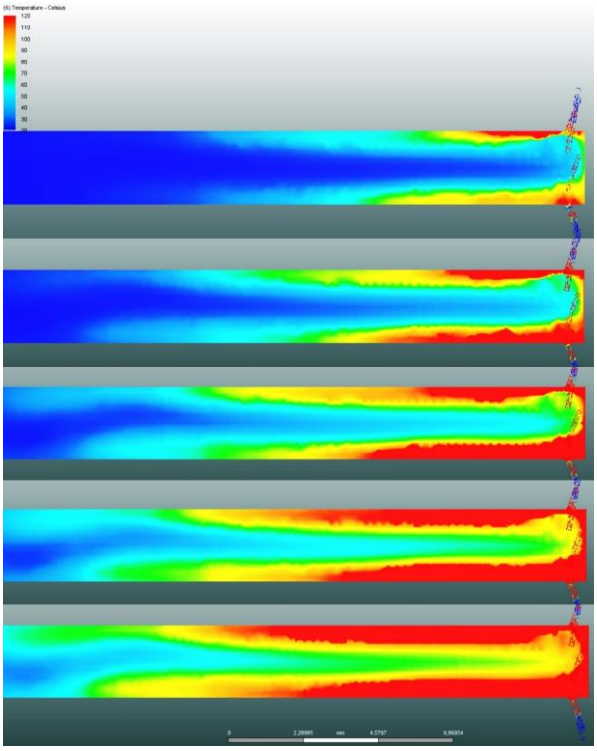

Figure 12 Time-dependent visualization of hot and cold airflow separation - Model 2 (30-Iteration intervals)

Figure 12 presents a time-dependent visualization of the separation of hot and cold airflow fractions in Model 2, depicted through a colour gradient at 30-iteration intervals. This iterative visualization effectively illustrates the separation process and the formation of a cold core, which facilitates the exit of the cold fraction through the centre of the cone valve at the tube's end. The simulation results in Figure 12 demonstrate that thermal separation within the vortex is effective, achieving a temperature difference of up to 100°C. A distinct cold core is observed near the inlet, though it gradually warms over time. Along the tube length, the disruption of the vortex structure coincides with the loss of a clearly defined cold core. Consistent with previous observations, the cyclone structure remains unstable in this model. Consequently, the simulation indicates that no significant separation of fractions is achieved at the tube's outlet.

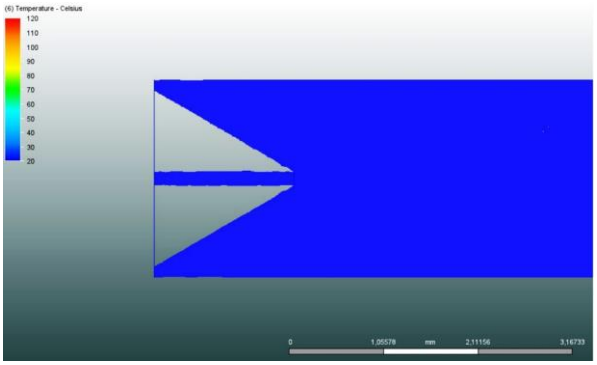

Figure 13 Temperature field with streamlines at the outlet and tube body - Model 2

Figure 13 presents a visualization of the temperature field using a colour gradient. Swirling motion initiated at the inlet leads to the progressive development of airflow fraction separation along the tube length, as evidenced by the time-dependent visualization in Figure 12. However, the simulation results in Figure 13 demonstrate that the desired separation effect is not achieved at the outlet.

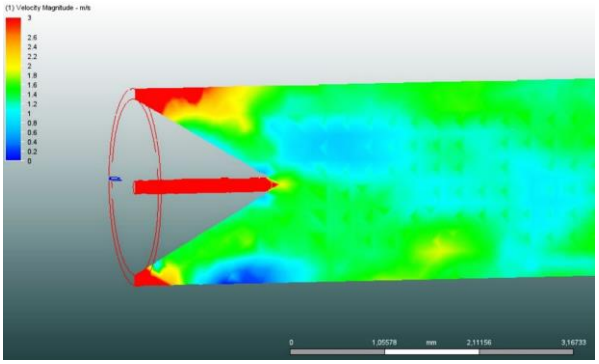

Figure 14 Velocity field with streamlines at the outlet and tube body - Model 2

„Figure 14 illustrates the velocity field distribution of airflow at the end and outlet of the vortex tube in Model 2, visualized using a colour gradient. A comparison of the simulation results and streamline visualizations from Figure 11 with the colour gradient representation in Figure 14 reveals a transition from intense swirling motion near the inlet to a diminished vortex at the tube's end, accompanied by an expected reduction in velocity. At the fraction outlets, airflow velocities approximate 3 m/s. Similar to the findings for

Model 1, these results indicate that optimizing inlet parameters remains essential to maximize the vortex effect in Model 2. The simulation outcomes provide valuable insights for further investigation of the proposed vortex tube geometries. These findings suggest that, with appropriate adjustment of the inlet medium parameters, the desired separation of airflow fractions can be achieved.

4 Conclusions

The aim of this study was to design a uniflow Ranque-Hilsch vortex tube (RHVT) model and conduct CFD simulations of the flow and temperature field based on existing mathematical relationships. The results of the first model indicated that the initially proposed geometry was unsuitable, leading to its modification and a change in the method of compressed air supply to the tube. The geometry design continued to follow the equations derived for counter-flow RHVTs, with simulations intended to verify their applicability to the uniflow configuration.

Based on the analysis of the simulation results, the following conclusions can be drawn:

- *Model 1*
  - The vortex effect was only partially achieved, with an insignificant temperature separation (≈1 °C).
  - The tube length obtained from the mathematical equations was too large, preventing the vortex motion from being sustained for a sufficient duration. As a result, premature mixing of the flow occurred before reaching the outlet, leading to heat dispersion and the loss of the desired Ranque-Hilsch effect.
- *Model 2*
  - By reducing the tube length by a factor of ten, new geometric parameters were obtained while still using the same mathematical equations.
  - The vortex effect was more pronounced, and temperature separation was achieved at an expected level (≈100 °C).

A comparison of the simulation results of both models suggests that achieving the Ranque-Hilsch effect in a uniflow RHVT is partially possible. However, the mathematical equations developed for counter-flow vortex tubes are not entirely suitable for designing a uniflow configuration capable of achieving the desired effect. The geometric parameters derived from these equations did not yield the expected results, indicating that a different optimization approach is required for uniflow RHVTs.

To achieve a more efficient uniflow RHVT design, experimental validation of various geometric configurations is necessary, either through further CFD simulations or physical experiments on laboratory models. Future research should focus on deriving specific mathematical relationships for uniflow RHVTs that better account for the flow dynamics and allow for a more precise design of the device.

5 The reference list

[1] KIZEK, J., HUDÁK, Ľ., JABLONSKÝ, G., DZURŇÁK, R., KARAKASH, Y., KÁŇA, M.: Analysis of the work of experimental equipment on the principle of the vortex tube, *Advance in Thermal Processes and Energy Transformation*, Vol. 2, No. 4, pp. 76-80, 2019. [CrossRef]

[2] TAKAHAMA, H. KAWAMURA, H., KATO, S., YOKOSAWA, H.: Performance characteristics of energy separation in a steam-operated vortex tube, *Int. J. Eng. Sci.*, Vol. 17, pp. 735–744, 1979. [CrossRef]

[3] SONI, Y.: *A parametric study of the Ranque-Hilsch tube.* PhD thesis. University of Idaho, 1973.

[4]. TESLA NIKOLA: *My Inventions: The Autobiography of Nikola Tesla.* Createspace Independent Publishing Platform, 10 December 2017.

[5] RANQUE, G.J.: *Method and apparatus for obtaining from a fluid under pressure two currents of fluid at different temperatures*, US Patent No. 1952281, March 1934.

[6] HILSCH, R.: The use of the expansion of gases in a centrifugal field as cooling process. *Rev. Sci. Instrum.*, Vol. 18, No. 2, pp. 108–113, 1947.

[7] THAKARE, H.R., MONDE, A., PAREKH, A.D.: Experimental, computational and optimization studies of temperature separation and flow physics of vortex tube: A review. *Renew. Sustain. Energy Rev.*, Vol. 52, pp. 1043–1071, 2015[CrossRef]

[8] LINDERSTRØM-LANG, C. U.: *Studies on transport of mass and energy in the vortex tubes. The significance of the secondary flow and its interaction with the tangential velocity distribution*. Risø National Laboratory. Denmark. Forskningscenter Risoe. Risoe-R, No. 248, 1971.

[9] WESTLEY, R.: *Optimum design of a Vortex Tube for achieving larger temperature drop ratios*. Cranfield College Note No. 30, College of Aeronautics, 1955.

[10] EIAMSA-ARD, S., PROMVONGE, P.: Review of Ranque–Hilsch effects in vortex tubes, *Renewable and Sustainable Energy Reviews*, Vol. 12, pp. 1822-1842, 2008. [CrossRef]

[11] DUTTA, T., SINHAMAHAPATRA, K.P., BANDYOPADHYAY, S.S.: Experimental and numerical investigation of energy separation in counterflow and uniflow vortex tubes, *Int. J. Refrig.*, Vol. 123, pp. 9-22, 2021. [CrossRef]

[12] BARWARI, R.R.I.: Effect of Changing Cone Valve Diameter on the performance of Uni-Flow Vortex Tube. *International Journal of Engineering and Innovative Technology*, Vol. 3, No. 2, pp. 237-240, 2013.

[13] KIRAN KUMAR RAO, K., SHATANAPPA, G., RAMESH, A., NAGA MALLESWARA RAO, G.: Fabrication and Experimental Analysis of Vortex Tube by Varying the Geometry and Material. *IOSR Journal of Mechanical and Civil Engineering*, Vol. 3, pp. 17-25, 2017.
[14] RANQUE M.G.: Method and apparatus for obtaining from a fluid under pressure two currents of fluid at different temperatures. US Patent No. 1952281, March 1934.
[15] GAO, C.: *Experimental study on the Ranque-Hilsch vortex tube*, [Phd Thesis 1 (Research TU/e /Graduation TU/e), Applied Physics and Science Education].:Technische Universiteit Eindhoven, 2005. [CrossRef]
[16] SONI, Y., THOMPSON, W.J.: Optimal design of the Ranque–Hilsch vortex tube, *Trans ASME J Heat Transfer*, Vol. 94, No. 2, pp. 316–317, 1975.
[17] RAISKII, Y.D., TUNKEL, L.E.: Influence of vortex-tube configuration and length on the process of energetic gas separation. *J. Eng. Phys. Thermophys.*, Vol. 27, No. 6, pp. 1578-1581, 1974.
[18] YILMAZ, M., KAYA, M., KARAGOZ, S., ERDOGAN, S.: A review on design criteria for vortex tubes, *Heat Mass Transfer.*, Vol. 45, pp. 13–632123, 2009. [CrossRef]
[19] DEVADE, K., PISE, A.: Parametric Review of Ranque-Hilsch Vortex Tube. *Am. J. Heat Mass Transf.*, Vol. 4, No. 3 pp. 115-145, 2017. [CrossRef]
[20] KIRMACI, V., KAYA, H.: Effects of working fluid, nozzle number, nozzle material and connection type on thermal performance of a Ranque–Hilsch vortex tube: A review, *Int. J. Refrig.*, Vol. 91, pp. 254-266, 2018. [CrossRef]
[21] Autodesk Inc. Knowledge Network. Autodesk CFD 2021. Tutorials. Assigning Boundary Conditions. [Online], Available: https://help.autodesk.com/view/SCDSE/2021/ENU/?guid=GUID-6F2E3547-E76A-4F13-8A7D-44A9BC971C53, [10 Jan 2021], 2021.
[22] Autodesk Inc. Knowledge Network. Autodesk CFD 2021. Tutorials. Turbulence. [Online], Available: https://help.autodesk.com/view/SCDSE/2021/ENU/?guid=GUID-E9E8ACA1-8D49-4A49-8A35-52DB1A2C3E5F, [10 Jan 2021], 2021.
[23] Autodesk Inc. Knowledge Network. Autodesk CFD 2021. Tutorials. Advection Schemes. [Online], Available: https://help.autodesk.com/view/SCDSE/2021/ENU/?guid=GUID-F691B334-CCE2-47E9-B6C4-21666712C163, [10 Jan 2021], 2021.

Acknowledgement
This article was supported by the Cultural and Educational Grant Agency of the Ministry of Education, Research, Development, and Youth of the Slovak Republic, through the project KEGA 024TUKE-4/ 2024.